Effects of screening on the Hofstadter butterfly

Vidar Gudmundsson
Science Institute, University of Iceland, Dunhaga 3, IS-107 Reykjavik, Iceland.

Rolf R. Gerhardts
Max-Planck-Institut für Festkörperforschung, Heisenbergstraße 1, D-70569 Stuttgart, Federal Republic of Germany
(February 1, 2008)

arXiv:cond-mat/9509064v1 12 Sep 1995

Abstract

We study, within the Hartree approximation, the effects of the electron-electron interaction on the energy spectrum of a two-dimensional electron gas in a perpendicular homogeneous magnetic field and a lateral superlattice potential with square symmetry. Due to the strong screening effects, the bandwidth of the Landau bands oscillates strongly with their filling. For short enough periods and strong enough modulation of the superlattice potential, the miniband structure of the Landau bands can be resolved in the thermodynamic density of states.

71.20.-b 73.20.Dx

Typeset using REVTEX

I. INTRODUCTION

The study of the characteristics of a two-dimensional electron gas (2DEG) in a homogeneous perpendicular quantizing magnetic field $\vec{B}$ and a lateral periodic superlattice potential has been revived, since due to recent technological developments it now is possible to manifacture such systems with controlable properties in semiconductor heterostructures. Measurements of the magnetotransport in superlattices weakly modulated in one or two directions have revealed novel oscillations in the conductivity, the Weiss oscillations, reflecting the commensurability of the cyclotron radius $R_c = l^2 k_F = v_F/\omega_c$ of the electrons at the Fermi energy $E_F = \hbar^2 k_F^2/(2m^*)$ and the modulation period L, $l = (c\hbar/eB)^{1/2}$ is the magnetic length. [1,2] The Weiss oscillations are superimposed on top of the Shubnikov-de Haas oscillations which are well known in homogeneous 2DEG's and caused by the commensurability of the Fermi wavelength λ_F and l.

Transport calculations have been able to explain the observed difference in the Weiss oscillatons for weakly 1D and 2D modulated superlattices in a strong magnetic field. [3] The periodic potential lifts the degeneracy of the Landau levels (LL's) leading to Landau bands (LB's) of oscillating width periodic in B^{-1}. The bandwidth is determined [4–8] by the commensurability of R_c and L.

The single-particle energy spectrum for this problem has been investigated by several researchers [9–14] culminating in Hofstadter's butterfly, [13] a graph showing the complicated self-similar splitting of a LB into minibands as a function of the magnetic flux through a unit cell of the lattice. The effects of the splitting of LB's into minibands has, to the best of our knowledge, not been observed directly in the currently common superlattices ($L \sim 300$ nm $n_s = 3\times10^{11}\,\mathrm{cm}^{-2}$) since usually several LB's are occupied, which may overlap near E_F. Transport calculations based on the Hofstadter energy spectrum and taking into account short-range impurity scattering have, however, succeeded in recovering all the observed features of the magnetotransport coefficients for large-period superlattices. [3] In the limit of a very high magnetic field the intricate gap structure of the Hofstadter butterfly is robust but long-range disorder tends to smear out the fine structure in the density of states. [15]

The Hofstadter butterfly is obtained in two complimentary but mathematically equivalent limits: [11] first, in a strong lattice potential and a weak magnetic field in the tight-binding method, [9,11,13] and, second, a weak periodic perturbation of Landau quantized 2DEG. [11,14,16] Both approaches deliver the so-called Harper's equation [9,11] determining the energy spectrum. The energy spectrum has been investigated in the intermediate region in the absence of collision broadening. The coupling of the LL's by the external periodic potential strongly reduces the original high symmetry of the Hofstadter spectrum but retains a very complicated subband structure. [17,18] It has been possible to transform the equation of motion, the Schrödinger equation, into a vectorial form reminiscent of Harper's equation, but exact under the

most general conditions and exhibiting chaos in the classical limit. [18]

All the above-mentioned theoretical investigations of the energy spectrum of a 2DEG in a periodic potential and a homogeneous perpendicular magnetic field have neglected the effects of the electron-electron interaction. In the present publication we initiate, within the Hartree approximation, the study of these effects on the electronic energy spectrum and the thermodynamic density of states.

II. MODEL

To describe the electrons in the conduction band of a lateral superlattice at the AlGaAs-GaAs interface in a constant perpendicular magnetic field $\vec{B} = B\hat{z}$ we employ a model of strictly two-dimensional electron gas (2DEG), with the three-dimensional charge density given by $-en_s(\vec{r})\delta(z)$, and $\vec{r} = (x, y)$. The orthogonal superlattice is spanned by the lattice vectors

$$\vec{R} = m\vec{l_1} + n\vec{l_2}, \quad n, m \in Z. \tag{1}$$

$\vec{l_1} = l_1\hat{x}$, and $\vec{l_2} = l_2\hat{y}$ are the primitive translations of the Bravais lattice $\mathcal{B}$. The corresponding reciprocal lattice $\mathcal{R}$ is spanned by

$$\vec{G} = G_1\vec{g}_1 + G_2\vec{g}_2, \quad G_1, G_2 \in Z, \tag{2}$$

where

$$\vec{g}_1 = 2\pi\frac{\hat{x}}{l_1}, \quad \vec{g}_2 = 2\pi\frac{\hat{y}}{l_2} \tag{3}$$

The external periodic potential the electrons are moving in is taken to be of the simple form

$$V(\vec{r}) = V_x\cos(g_1x) + V_y\cos(g_2y). \tag{4}$$

The electron-electron interaction is included in the Hartree approximation (HA) leading to the effective single-electron Hamiltonian

$$H = H_0 + V_H(\vec{r}) + V(\vec{r}), \tag{5}$$

where $V_H(\vec{r})$ is the effective potential in a medium with a dielectric constant κ,

$$V_H(\vec{r}) = \frac{e^2}{\kappa}\int_{R^2} d^2r' \; \frac{n_s(\vec{r}\,') - n_b}{|\vec{r} - \vec{r}\,'|} \quad , \tag{6}$$

felt be each electron and caused by the total charge density of the 2DEG, $-en_s(\vec{r})$, and the neutralizing background charge density $+en_b = +e\langle n_s(\vec{r})\rangle$.

The periodic external potential $V(\vec{r})$ and the constant external magnetic field imply that all physical quantities of the noninteracting system are periodic with respect to translations of $\vec{R} \in \mathcal{B}$. Since the Coulomb interaction is

given by a central potential between pairs of electrons, the periodicity of the system is not broken by the electron-electron interaction. The periodicity of the Hartree potential (6) follows from that of $n_s(\vec{r})$.

The translation operator

$$T(\vec{R}) = \exp\left(-\frac{i}{\hbar}\vec{R}\cdot\vec{p}\right), \tag{7}$$

where $\vec{p}$ is the momentum canonical to $\vec{r}$, does not commute with H_0, $[T(\vec{R}), H_0] \neq 0$. Due to the presence of the vector potential $\vec{A}$ in H_0,

$$H_0 = \frac{1}{2m}\left(\vec{p} + \frac{e}{c}\vec{A}\right)^2, \quad \vec{B} = \vec{\nabla}\times\vec{A} \tag{8}$$

an additional gauge transformation is necessary. Defining the magnetotranslation

$$S(\vec{R}) = \exp\left(\frac{ie}{\hbar c}\chi\right)T(\vec{R}), \tag{9}$$

where χ is obtained from $T^{-1}\vec{A}T = \vec{A} + \vec{\nabla}\chi$, we have for the mechanical momentum $\vec{\pi} = \vec{p} + (e/c)\vec{A}$ and the position $\vec{r}$

$$\begin{aligned} S^{-1}(\vec{R})\vec{r}S(\vec{R}) &= \vec{r} + \vec{R} \\ S^{-1}(\vec{R})\vec{\pi}S(\vec{R}) &= \vec{\pi}. \end{aligned} \tag{10}$$

The Hamiltonian H is thus invariant with respect to the magnetotranslations, $[S(\vec{R}), H] = 0$.

H_0 defines the natural length and frequency scales for the system by the magnetic length l and the cyclotron frequency ω_c

$$l = \sqrt{\frac{c\hbar}{eB}}, \quad \omega_c = \frac{eB}{mc}. \tag{11}$$

Generally the magnetotranslations (9) do not commute, $[S(\vec{R}_1), S(\vec{R}_2)] \neq 0$, expressing the fact that l is not commensurate with the lattice. But if an integer number of flux quanta $\Phi_0 = (hc/e)$ flows through the lattice unit cell $\vec{l}_1 \times \vec{l}_2$, then $[S(\vec{R}_1), S(\vec{R}_2)] = 0$ and the magnetic field assumes the values

$$B = g_l \frac{\Phi_0}{|\vec{l}_1 \times \vec{l}_2|}, \quad g_l \in Z. \tag{12}$$

For these values of B the magnetotranslations (9) of the lattice vectors commute with each other, with H, and also with H_0. Thus, the known eigenvectors of H_0 can be chosen to be also eigenvectors of the unitary magnetotranslations with simple eigenvalues

$$\begin{aligned} S(\vec{l}_1)\psi &= e^{i\theta_1}\psi \\ S(\vec{l}_2)\psi &= e^{i\theta_2}\psi, \quad \theta_i \in [-\pi, \pi]. \end{aligned} \tag{13}$$

The above eigenequations can be reinterpreted as periodic boundary conditions for the wave functions within one unit cell of $\mathcal{B}$, and the eigenfunctions form a complete basis for each pair of phase angles (θ_1, θ_2).

Here we use the symmetric basis functions constructed by Ferrari [19] and used by Silberbauer. [20,21] A finer lattice with only one flux quantum through a unit cell is defined by the primitive vectors

$$\vec{c} = \frac{\vec{l_1}}{p}, \quad \vec{d} = \frac{\vec{l_2}}{q}, \quad pq = g_l, p, q \in N. \tag{14}$$

With the symmetric gauge $\vec{A} = (B/2)(-y, x)$ the functions

$$\phi^{\mu\nu}_{n_l}(\vec{r}) = \frac{1}{\sqrt{pq}} \sum_{m,n=-\infty}^{\infty} \left[S(\vec{c})e^{-i\mu}\right]^m \left[S(\vec{d})e^{-i\nu}\right]^n \phi_{n_l}(\vec{r}), \tag{15}$$

where

$$\begin{aligned}
\mu &= \frac{\theta_1 + 2\pi n_1}{p}, \qquad n_1 \in I_1 = \{0, \ldots p-1\} \\
\nu &= \frac{\theta_2 + 2\pi n_2}{q}, \qquad n_2 \in I_2 = \{0, \ldots q-1\} \\
\phi_{n_l}(\vec{r}) &= \frac{1}{\sqrt{2\pi n_l! l^2}} \left(\frac{x+iy}{\sqrt{2}l}\right)^{n_l} \exp\left(-\frac{r^2}{4l^2}\right), \quad n_l = 0, 1, 2 \ldots,
\end{aligned} \tag{16}$$

form a complete orthogonal basis in the Hilbert space $\mathcal{H}_{\theta_1\theta_2}$ if $(\mu, \nu) \neq (\pi, \pi)$ for all $(n_1, n_2) \in I_1 \times I_2$. The norm of the $\phi^{\mu\nu}_{n_l}$ can be shown to be

$$||\phi^{\mu\nu}_{n_l}||^2 = \sum_{m,n=-\infty}^{\infty} (-1)^{mn} e^{i(\mu m + \nu n)} \exp\left(-\frac{1}{4l^2}|n\vec{c} + m\vec{d}|^2\right) , \tag{17}$$

and they have on the finer lattice the Bloch-type property

$$S(\vec{c})\phi^{\mu\nu}_{n_l} = e^{i\mu}\phi^{\mu\nu}_{n_l}, \quad S(\vec{d})\phi^{\mu\nu}_{n_l} = e^{i\nu}\phi^{\mu\nu}_{n_l}. \tag{18}$$

In order to utilize the Ferrari-basis (15) $\{\phi_\alpha\}$, each element of which satisfies

$$H_0\phi_\alpha = E_\alpha\phi_\alpha, \quad \alpha = (\mu, \nu, n_l), \tag{19}$$

to find the energy spectrum $\{\epsilon_\alpha\}$ and the eigen functions $\{\psi_\alpha\}$ of H,

$$H\psi_\alpha = (H_0 + V + V_H)\psi_\alpha = \epsilon_\alpha\psi_\alpha, \tag{20}$$

we need the matrix elements of the external periodic potential $V(\vec{r})$ and the Hartree potential (6) in that basis. Both $V(\vec{r})$ and $V_H(\vec{r})$ are periodic with respect to $\vec{R} \in \mathcal{B}$ and can be expressed in terms of a Fourier series

$$V(\vec{r}) = \sum_{\vec{G}\in\mathcal{R}} V(\vec{G})e^{i\vec{G}\cdot\vec{r}}, \tag{21}$$

with the Fourier coefficients given by

$$V(\vec{G}) = \frac{1}{A}\int_A d^2r\, V(\vec{r}) e^{-i\vec{r}\cdot\vec{G}}. \tag{22}$$

Here A stands both for the unit cell in $\mathcal{B}$ and it's area $|\vec{l}_1 \times \vec{l}_2|$. The task of deriving the matrix elements of the external potentials is thus reduced to finding the matrix element of the Fourier phase factor. This has been accomplished by Silberbauer showing that the matrix elements can be expressed as rapidly converging series of simple analytic functions. [20,21] The result is reproduced here, correcting a simple typographical error in one of the sources [20]

$$\langle n_1' n_2' n_l' | e^{i\vec{G}\cdot\vec{r}} | n_1 n_2 n_l \rangle = G^{n_l' n_l}(G) T^{n_1' n_2'}_{n_1 n_2}(G) \frac{e^{-\frac{|G|^2 l^2}{4}}}{||\phi^{n_1' n_2'}_{n_l'}||\, ||\phi^{n_1 n_2}_{n_l}||}, \tag{23}$$

where

$$T^{n_1' n_2'}_{n_1 n_2}(G) = \sum_{\Lambda\Omega=-\infty}^{\infty} (-1)^{\Lambda\Omega} e^{(\mu'\Lambda+\nu'\Omega)} \exp\left\{ -\frac{i}{2} G(\Lambda c + \Omega d)^* - \frac{|\Lambda c + \Omega d|^2}{4l^2} \right\} \tag{24}$$

and

$$G^{n_l' n_l}(G) = \begin{cases} \sqrt{\frac{n_l}{n_l'}} e^{-\frac{|G|^2 l^2}{4}} \left(\frac{iG^* l}{\sqrt{2}}\right)^{n_l' - n_l} L_{n_l}^{n_l' - n_l}\left(\frac{|G|^2 l^2}{2}\right) & \text{if} \quad n_l' \geq n_l \\ \sqrt{\frac{n_l'}{n_l}} e^{-\frac{|G|^2 l^2}{4}} \left(\frac{iGl}{\sqrt{2}}\right)^{n_l - n_l'} L_{n_l'}^{n_l - n_l'}\left(\frac{|G|^2 l^2}{2}\right) & \text{if} \quad n_l \geq n_l' \end{cases} \tag{25}$$

Here a complex notation, $G = G_1|\vec{g}_1| + iG_2|\vec{g}_2|$ etc., has been used for the vectors $\vec{G}$, Eq. (2), and similarly for $\vec{c}$, and $\vec{d}$, Eq. (14). L_m^n are the associate Laguerre polynomials. Furthermore, the matrix elements $T^{n_1' n_2'}_{n_1 n_2}(G)$ vanish unless $G_1 = n_1' - n_1 - Mp$ and $G_2 = n_2' - n_2 - Nq$ for some $M, N \in Z$.

The Fourier coefficients for the Hartree potential are

$$V_H(\vec{G}) = \begin{cases} 2\pi \frac{e^2}{\kappa|\vec{G}|} \Delta n_s(\vec{G}) & \text{if} \quad \vec{G} \neq 0 \\ 0 & \text{if} \quad \vec{G} = 0 \end{cases}, \tag{26}$$

where

$$\Delta n_s(\vec{G}) = \frac{1}{A}\int_A d^2r'\ \{n_s(\vec{r}\,') - n_b\}\, e^{-i\vec{r}\,'\cdot\vec{G}}. \tag{27}$$

The charge neutrality of the system removes the singularity of the Coulomb interaction for $\vec{G} = 0$.

To complete the Hartree set of equations (4), (5), (6), and (8) the electron density is written in terms of $\{\epsilon_\alpha\}$ and $\{\psi_\alpha\}$ as

$$n_s(\vec{r}) = \frac{1}{4\pi^2} \sum_\alpha \int_{-\pi}^{\pi} d\theta_1 d\theta_2\, f(\epsilon_\alpha - \mu) |\psi_\alpha(\vec{r})|^2, \tag{28}$$

where f is the equilibrium Fermi distribution and μ is the chemical potential. This set of Hartree equations has to be solved iteratively together with the condition that the average electron density $n_s = N_s/A$ is constant and determines the chemical potential μ. N_s is the number of electrons per unit cell with area A in $\mathcal{B}$.

III. RESULTS

The Coulomb interaction couples directly the subbands of a particular LL and the subbands of different LL's via the matrix elements (23). The matrix elements with states of different phase angles (θ_1, θ_2) do all vanish, so that the Hartree Hamiltonian can be diagonalized for each pair (θ_1, θ_2) separately. However, the states for a given set of phase angles depend on the states of all other phase angles via the Hartree potential (6) and the density $n_s(\vec{r})$ (28). The self-consistent model described in the above section can be used to evaluate the energy spectra $\{\epsilon_\alpha\}$ and the wavefunctions $\{\psi_\alpha\}$ for a wide variety of modulation strengths V_x and V_y and values of the magnetic field B by selecting the appropriate size of the basis, H is diagonalized in. If only the basis states in the same LL are taken into account, the modulation strength is irrelevant since it can be factored out of the Hamiltonian matrix. In this situation, corresponding to the usual discussion of Hofstadter's butterfly on the basis of Harper's equation, a highly symmetric energy spectrum is expected. Of course, this restricted model is only appropriate for describing a system with very weak modulation (as compared with the inter-Landau-level energy spacing $\hbar\omega_c$). In the following, parameters appropriate for GaAs have been used, i.e. $m^* = 0.067m_0$, $\kappa = 12.4$, and the spin degree of freedom has been completely neglected since the exchange force is not accounted for in the interaction between the electrons. The superlattice is selected to have square symmetry, $l_1 = l_2 = L$, and $V_x = V_y = V_0$, to comply with the usual experimental conditions, even though the Ferrari-basis is applicable for a much more complicated unit cell. [19–21]

The iteration of the Hartree equations (4), (5), (6), and (8) has been accomplished by specifying an initial electron density that is then used to find the Hartree potential (6). Subsequently the Hamiltonian (5) is diagonalized yielding $\{\epsilon_\alpha\}$ and $\{\psi_\alpha\}$ that are in turn used to derive a new density (28). In order to guarantee convergence the speed of the iteration process is reduced by using only 10% of the new densty and 90% of the density from the former iteraction cycle. The convergence is considered completed when the integrated rms deviations of the density from two subsequent cycles falls below 0.01% of N_s. Clearly the convergence rate depends on modulation stength of the external potential (4), the filling factor ν and the temperature T. Commonly for the following parameters we need between 15 and 30 cycles to attain the specified accuracy. For the ground state properties the evaluation of the wave functions can be avoided by combining equations (27) and (28) and thus write the Fourier transformed density entirely as a function of the analytically known matrix elements (23).

The energy spectrum for the case of four flux quanta Φ_0 piercing the unit cell of a Hartree interacting 2DEG periodically modulated with $L = 50$ nm is shown in Fig. 1. The dimensionless magnetic flux is thus, $\Phi/\Phi_0 = pq = 4$, which translates into a magnetic field of $B \approx 6.617$ T and $\hbar\omega_c \approx 11.43$ meV. Due to the strong modulation of the periodic potential (4), $V_0 = 4.0$ meV,

and the low temperature $T = 0.2\,\mathrm{K}$, four separate subbands of the lowest LB are resolved, which are centered about $E = \hbar\omega_c/2 \approx 5.7\,\mathrm{meV}$. The electronic density is very low, $N_s = 0.25$ being the average number of electrons per unit cell. The chemical potential $\mu = 2.38\,\mathrm{meV}$ is lying in the lowest subband which has a very slight dispersion as function of the phase angles θ_1 and θ_2. This is a manifestation of the familiar pinning effect observed earlier in many different systems. [22,23] The relatively weak screening (judged from the spread of the minibands $\leq 2V_0$) is strongest in the subband where μ is situated. The next LB is centered around $E = 3\hbar\omega_c/2 \approx 17.1\,\mathrm{meV}$ and has a much weaker dispersion than the first one. The vanishing overlap of the LB's leads to an approximate electron-hole symmetry between the cases $N_s = 0.25$ and $N_s = 3.75$, since the (average) filling factor $\nu = 1$ is reached for $N_s = 4$. Note however that, e.g. for $N_s = 0.25$, the energy spectrum is not symmetric around the mean energy, in contrast to the case of the noninteracting electrons. This approximate symmetry can also be seen in Fig. 2 in which the self-consistent potential $V_{sc}(\vec{r}) = V_H(\vec{r}) + V(\vec{r})$ for $pq = 6$ has been depicted. Here the intersection of the shifted chemical potential $\mu - \hbar\omega_c/2$ with V_{sc} projected onto the basis of the graph is also shown. For $N_s = 0.25$ (Fig. 2a) the 2DEG forms isolated lakes near the minima of V_{sc}. The complimentary case, $N_s = 5.75$, is depicted in Fig. 2c, where the empty states of the first LB, "the holes," are isolated near the maxima of the potential. The transition between these two regions is seen in Fig. 2b, where traditionally, i.e. in a semi classical picture, neither the electrons nor the holes are thought to form closed orbits. The screening is so strong for this last case (corresponding to $\nu = 1/2$) that V_{sc} is almost flat. As stated earlier, the symmetry is only approximate, since the states of the second LB are mixed into the states of the first one by the interaction. The potentials are thus not identical for the complimentary cases of $N_s = 0.25$ and 5.75, and the transition between the two regions does not happen exactly at $N_s = 3.00$. The self-consistent densities of the electrons for the cases $N_s = 0.25$ and $N_s = 5.75$ is shown in Fig. 3, underlining clearly the near isolation of the electrons in the minima of V_{sc} when $N_s = 0.25$. In Fig. 4 we compare the self-consistent density $n_s(\vec{r})$ with the density of the non interacting 2DEG for $N_s = 3.00$. For $pq = 6$ the screening is at its maximum strength but due to the strong modulation $V_0 = 4.0\,\mathrm{meV}$ the interaction only causes a moderate flattening of the density.

The strong screening encountered in Fig. 2 for the $pq = 6$ case is even more drastic for a superlattice potential $V(\vec{r})$ with a longer period and weaker modulation as can be observed from Fig. 5 when $L = 200\,\mathrm{nm}$ and $V_0 = 0.5\,\mathrm{meV}$. Here the width and the location of each subband of the lowest LB is shown as a function of N_s, the location of the chemical potential is also indicated. Even though the temperature is quite low, $T = 0.1\,\mathrm{K}$, the Coulomb interaction between the electrons is very effective in screening the superlattice potential and collapsing the subbands into an almost degenerate LL around $N_s \sim 3$ corresponding to $\nu \sim 1/2$. For an integer filling factor of the order of unity ($N_s \sim 6$) the screening is as expected very weak. [22]

The upper panel of Fig. 5 shows the path of the chemical potential μ through the subbands as a function of the average filling factor ν or N_s when the electrons do not interact. The fine structure of μ leads to a peak structure of the (dimensionlessly written) thermodynamic density of states (TDOS)

$$D_T = l^2 \hbar\omega_c \left(\frac{\partial n_s}{\partial \mu}\right)_{TB}, \quad n_s = \langle n_s(\vec{r})\rangle \tag{29}$$

whenever μ crosses a subband. The strong screening in the case of the interacting 2DEG (the lower panel of Fig. 5) results in only one peak in D_T, in which no fine structure is resolved. The corresponding information is shown for four different cases in Fig. 6, $pq = 2, 3, 4, 6$, identifiable from the number of subbands appearing in each figure. Here the period is short, $L = 50\,\mathrm{nm}$, the modulation strong, $V_0 = 4.0\,\mathrm{meV}$, and $T = 1.0\,\mathrm{K}$. However only one LL is used in the calculation, so that the results apply to the case of a weak superlattice potential. Here the electron-hole symmetry is exact, as is reflected in each of the four cases by the point symmetry of the subband structure around the chemical potential μ at half filling. The screening is strongly dependent on the total number of states in a lattice unit cell and the average filling factor. It is therefore, strongest for $pq = 6$ when maximum six electrons can occupy the lowest Landau level in the unit cell and when the LB is half filled, $N_s = 3$. The thermodynamic density of states D_T, Eq. (29), for the corresponding cases is shown in Fig. 7. Clearly the strong screening in the $pq = 6$ case obscures the fine structure in D_T leading to only one pronounced peak. The subbands in the other cases turn up as separate peaks in D_T. The calculation has been repeated for the same parameters but one more Landau level resulting in qualitatively the same picture. The electron-hole symmetry is then only approximate with the largest deviation for $pq = 2, 3$, but the resolution of the peaks in D_T is unchanged.

The Hofstadter butterfly should be recovered when the calculation is performed for $N_s = 0$ and only one LL, and if the width and location of the subbands are plotted as functions of the inverse of the number of magnetic flux quanta through a unit cell of the lattice, i.e. of $\Phi_0/\Phi = 1/(pq)$. In addition, all energies have to be scaled according to: $E \to (E - \hbar\omega_c/2)/V_0$. For interacting electrons the number of electrons per unit cell N_s, or the average filling factor of the LB turns out to be a new parameter controlling the bandstructure. We therefore, present in Fig. 8 the subband structure for the four inverse fluxes $1/(pq) = 1/2, 1/3, 1/4, 1/6$ in the four cases $N_s = 0.00, 0.25, 1.00, 1.50$ together with the location of the chemical potential μ (except for $N_s = 0.00$, where it is irrelevant). For low density, say $N_s = 0.25$, the subband structure is almost symmetric around the energy zero, like in the noninteracting case, but the subbands become quite asymmetric for a higher density of electrons. For the short-period superlattice studied here, and for a low density of electrons, the essential gap structure does survive in the presence of interaction. The presentation in each of the subfigures of Fig. 8 corresponds to the experimental procedure of keeping the density of electrons fixed but changing the magnetic field. Another way

to investigate the screening is to keep the average filling factor ν constant but vary the magnetic field and, thus, also the average density of the 2DEG. Fig. 9 compares the subband structures for $1/(pq) = 1/2, 1/3, 1/4, 1/6$ and $\nu = 1/2$ with the complete Hofstadter butterfly. Here the energies have been scaled with the factor $(E - \hbar\omega_c/2)\exp\{(\pi l/L)^2\}/V_0$ so that the results can be directly compared with an earlier calculation of the Hofstadter spectrum. [3] The energy spectrum in the interacting case shows an overall reduction in dispersion or bandwidth due to the strong screening that is most effective for large flux and large number of available states. The bandwidths of the subbands for the interacting case has been evaluated here on a discrete lattice in the (θ_1, θ_2)-plane without attempting an interpolation between the lattice points; thus, the actual bandwidths can be larger by a small percentage of the widths shown. This effect explains why the bands for the even denominators in Fig. 8 for $N_s = 0$ are not touching.

IV. SUMMARY

In an interacting 2DEG subject to a superlattice potential and a homogeneous perpendicular magnetic field not only the magnetic flux through a unit cell but also the density of electrons determines the complicated splitting of the Landau bands into subbands. We have shown that in the Hartree approximation the essential gap structure of the energy spectrum remains, although the screening leads to a quenching of the Hofstadter butterfly at small values of the inverse flux (see Fig. 8). The symmetry of the butterfly is also lowered by the coupling to higher LL's due to increased strength of the periodic potential, as has already been discussed by other authors. [17,18] For periods around $L = 200\,\mathrm{nm}$ (currently attainable in experiments on superlattices) the 2DEG can effectively screen the periodic potential even for a very low density n_s so that only one or two Landau bands are partly occupied. Only at shorter lattice constants ($L < 100\,\mathrm{nm}$) and thus much higher magnetic fields we can, on the basis of our Hartree calculation, expect the subband structure to be resolvable in experiments, when n_s is maintained low enough. These predictions are made on the basis of the calculated energy spectrum and the structure observed in the thermodynamic density of states D_T, see Eq. (29). The transport coefficients do not depend on D_T in any simple way, and may be more sensitive to the subband structure of the energy spectrum. [3] In addition, the collision broadening due to impurities and inhomogeneities has to be considered, especially, when the electronic density is very low. [3,24,15]

It is to be expected that the inclusion of exchange and correlation effects may lead to more dramatic changes in the energy spectrum than the direct interaction considered in the Hartree approximation. One might even expect rearrangement of the bands or the occurence of spin-density waves. [25,23,26] A reliable procedure for the treatment of exchange and correlation effects in the 2DEG in a strong magnetic field and a lateral superlattice is, however, at present not available. Therefore we have restricted our investigation of the

electron-electron interaction effects by considering the Hartree approximation, which is expected to yield a qualitatively correct description of the dominant screening effects in inhomogeneous electron systems.

In order to keep the computational efforts in reasonable limits, we have restricted our calculations to a few characteristic values of the magnetic field. Our results indicate in which manner screening effects will change the overall appearence of the Hofstadter energy spectrum. Unfortunately, there is no simple way to extrapolate from these special values to arbitrary rational numbers of flux quanta per unit cell. For a more detailed comparison with the energy spectrum of the noninteracting case, further studies using a much denser set of flux values are desirable. However, the answer of the interesting question, whether the self-similarity of the Hofstadter butterfly survives in the presence of the mutual Coulomb interactions between the electrons, at least within the Hartree approximation, demands an amount of computational work which seems at present unfeasible. On the other hand, from the experimental point of view these details of the energy spectrum seem not to be accessible anyway. The challenge for the near future is to resolve the most prominent gaps of the energy spectrum experimentally.

ACKNOWLEDGMENTS

We are grateful to Behnam Farid for a critical reading of the manuscript. This research was supported in part by the Icelandic Natural Science Foundation, the University of Iceland Research Fund, and a NATO collaborative research Grant No. CRG 921204.

REFERENCES

[1] R. R. Gerhardts, D. Weiss, and K. v. Klitzing, Phys. Rev. Lett. **62**, 1173 (1989).

[2] D. Weiss, K. v. Klitzing, K. Ploog, and G. Weimann, Europhys. Lett. **8**, 179 (1989), see also in *High Magnetic Fields in Semiconductor Physics II*, edited by G. Landwehr, Springer Series in Solid-State Sciences Vol. **87** (Springer-Verlag, Berlin 1989), p. 357.

[3] D. Pfannkuche and R. Gerhardts, Phys. Rev. B **46**, 12606 (1992).

[4] R. R. Gerhardts and C. Zhang, Phys. Rev. Lett. **64**, 1473 (1990), surf. Sci. **229**, 92 (1990).

[5] C. Zhang and R. R. Gerhardts, Phys. Rev. B **41**, 12850 (1990).

[6] R. W. Winkler, J. P. Kotthaus, and K. Ploog, Phys. Rev. Lett. **62**, 1177 (1989).

[7] C. W. J. Beenakker, Phys. Rev. Lett. **62**, 2020 (1989).

[8] P. Vasilopoulos and F. Peeters, Phys. Rev. Lett. **63**, 2120 (1989), surf. Sci. **229**, 96 (1990).

[9] P. G. Harper, Proc. Phys. Soc (London) **A68**, 874 (1955).

[10] M. Y. Azbel', Sov. Phys. JETP **19**, 634 (1964), [Zh. Eksp. Teor. Fiz. **46**, 929 (1964)].

[11] D. Langbein, Phys. Rev. **180**, 633 (1969).

[12] A. Rauh, phys. stat. sol. (b) **69**, K9 (1975).

[13] R. D. Hofstadter, Phys. Rev. B **14**, 2239 (1976).

[14] D. J. Thouless, in *The Quantum Hall Effect*, *Graduate Texts in Contemporary Physics*, edited by R. Prange and S. Girvin (Springer-Verlag, New York, 1987), p. 101.

[15] U. Wulf and A. H. MacDonald, Phys. Rev B **47**, 6566 (1993).

[16] N. Usov, Sov. Phys. JETP **67**, 2565 (1988), [Zh. Eksp. Teor. Fiz. **94**, 305 (1988)].

[17] O. Kühn, P. E. Selbmann, V. Fessatidis, and H. L. Cui, J. Phys. C **5**, 8225 (1993).

[18] G. Petschel and T. Geisel, Phys. Rev. Lett. **71**, 239 (1993).

[19] R. Ferrari, Phys. Rev. B **42**, 4598 (1990).

[20] H. Silberbauer, J. Phys. C **4**, 7355 (1992).

[21] H. Silberbauer, Ph.D. thesis, University of Regensburg, 1994.

[22] U. Wulf, V. Gudmundsson, and R. Gerhardts, Phys. Rev. B **38**, 4218 (1988).

[23] A. Manolescu and R. R. Gerhardts, Phys. Rev. B **51**, 1703 (1995).

[24] P. Vasilopoulos and F. Peeters, Physica Scripta **T39**, 177 (1991).

[25] V. Gudmundsson and G. Pálsson, Physica Scripta T **54**, 92 (1994).

[26] D. Pfannkuche, V. Gudmundsson, and P. Maksym, Phys. Rev. B **47**, 2244 (1993).

FIGURES

FIG. 1. The dispersion of the four minibands of the lowest Landau level in the energy spectrum of the Hartree interacting 2DEG as a function of the phases θ_1 and θ_2 when four flux quanta of the magnetic field pierce a rectangular unit lattice cell ($p = q = 2$). $L_x = L_y = L = 50$ nm, $T = 0.2$ K, $V_x = V_y = V_0 = 4.0$ meV, $N_s = 0.25$, and $\mu = 2.38$ meV. Two Landau levels are included in the calculation.

FIG. 2. The self-consistent potential $V_{sc}(\vec{r}) = V_H(\vec{r}) + V(\vec{r})$ in a unit lattice cell for (a) $N_s = 0.25$, (b) $N_s = 3.00$, and (c) $N_s = 5.75$. The intersection of the chemical potential $\mu - \hbar\omega_c/2$ and V_{sc} is projected on the base and $\mu - \hbar\omega_c/2$ is shown in the upper right corner of each subfigure in meV. $p = 2$, $q = 3$, $L = 50$ nm, $T = 1.0$ K, $V_0 = 4.0$ meV. Two Landau levels are included in the calculation.

FIG. 3. The electron density $n_s(\vec{r})$ (nm^{-2}) in a unit lattice cell for (a) $N_s = 0.25$, and (b) $N_s = 5.75$. Contours of $n_s(\vec{r})$ are shown at the base. $p = 2$, $q = 3$, $L = 50$ nm, $T = 1.0$ K, $V_0 = 4.0$ meV. Two Landau levels are included in the calculation.

FIG. 4. The electron density $n_s(\vec{r})$ (nm^{-2}) in a unit lattice cell for $N_s = 3.00$. (a) Non interacting, and (b) Hartree interacting 2DEG. Contours of $n_s(\vec{r})$ are shown at the base. Same scales are used in both cases. $p = 2$, $q = 3$, $L = 50$ nm, $T = 1.0$ K, $V_0 = 4.0$ meV. Two Landau levels are included in the calculation.

FIG. 5. The bandwidth of the minibands of the lowest Landau band as a function of the number of electrons per unit cell N_s for a noninteracting 2DEG (upper) and a Hartree interacting 2DEG (lower). The chemical potential μ is noted by a continuous curve. $L = 200$ nm, $T = 0.1$ K, $V_0 = 0.5$ meV, $p = 2$, and $q = 3$. Two Landau levels are included in the calculation.

FIG. 6. The bandwidth of the minibands of the lowest Landau band as a function of the number of electrons per unit cell N_s for a Hartree interacting 2DEG and ($p = 1$, $q = 2$) (upper left), ($p = 1$, $q = 3$) (upper right), ($p = 2$, $q = 2$) (lower left), and ($p = 2$, $q = 3$) (lower right). The chemical potential μ is noted by a continuous curve. $L = 50$ nm, $T = 1.0$ K, $V_0 = 4.0$ meV. One Landau level is included in the calculation.

FIG. 7. The thermodynamic density of states $l^2\hbar\omega_c(\partial n_s/\partial\mu)_{TB}$ as a function of the dimensionless inverse magnetic flux through a unit cell $1/pq$ and N_s. $L = 50$ nm, $T = 1.0$ K, $V_0 = 4.0$ meV. One Landau level is included in the Hartree calculation.

FIG. 8. The scaled bandwidth of the subbands of the lowest Landau band $(E - \hbar\omega_c/2)/V_0$ as function of the dimensionless inverse magnetic flux $1/pq$ for $N_s = 0.00$ (upper left), $N_s = 0.25$ (upper right), $N_s = 1.00$ (lower left), and $N_s = 1.50$ (lower right). The chemical potential μ is noted by crosses. $L = 50$ nm, $T = 1.0$ K, $V_0 = 4.0$ meV. One Landau level is included in the Hartree calculation.

FIG. 9. The scaled bandwidth $(E - \hbar\omega_c/2)\exp\{(\pi l/L)^2\}/V_0$ of the subbands of the lowest Landau band as function of the dimensionless inverse magnetic flux $1/pq$ for the Hartree interacting 2DEG with $\nu = 1/2$ (left), and for the noninteracting 2DEG (right), the Hofstadter butterfly. One Landau level is included in the Hartree calculation. In the left subfigure the 6 LB's for the case $pq = 6$ can not all be resolved due to vanishing band gaps. The parameters used for the left subfigure are: $L = 50\,\mathrm{nm}$, $T = 1.0\,\mathrm{K}$, $V_0 = 4.0\,\mathrm{meV}$.

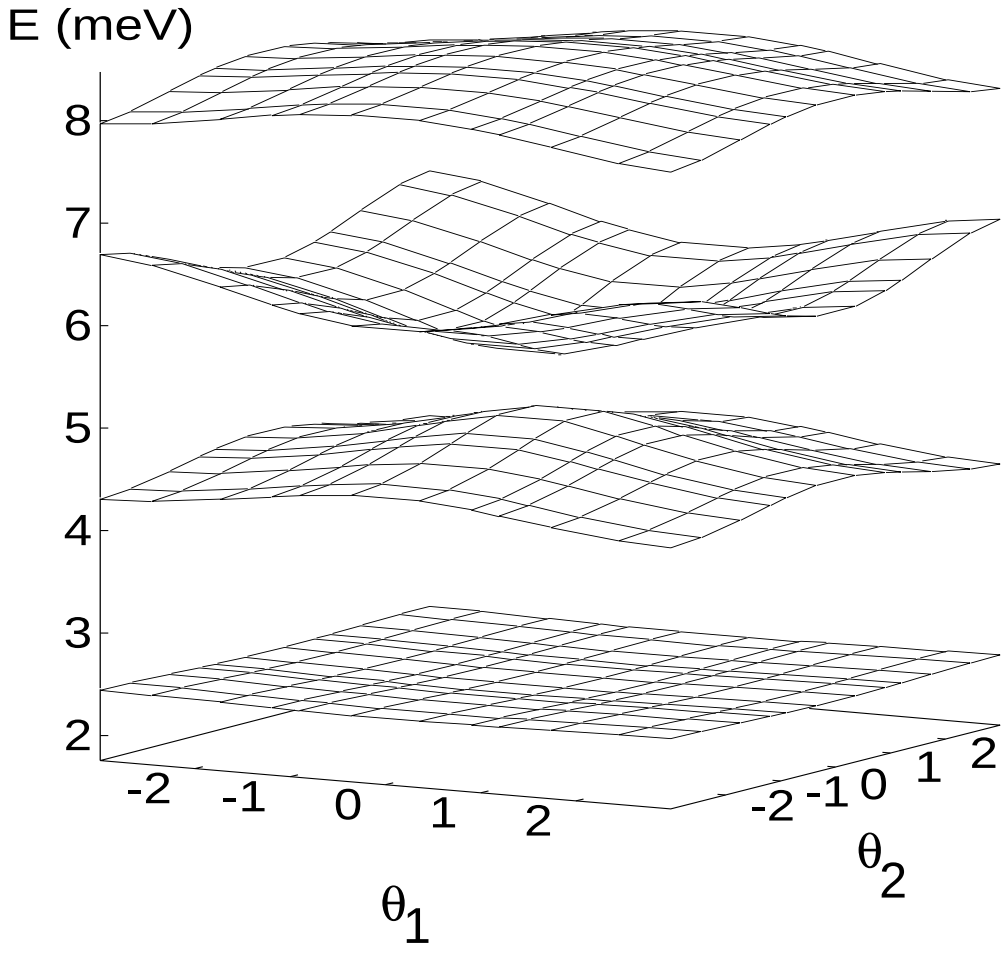

Gudmundsson, Fig. 1

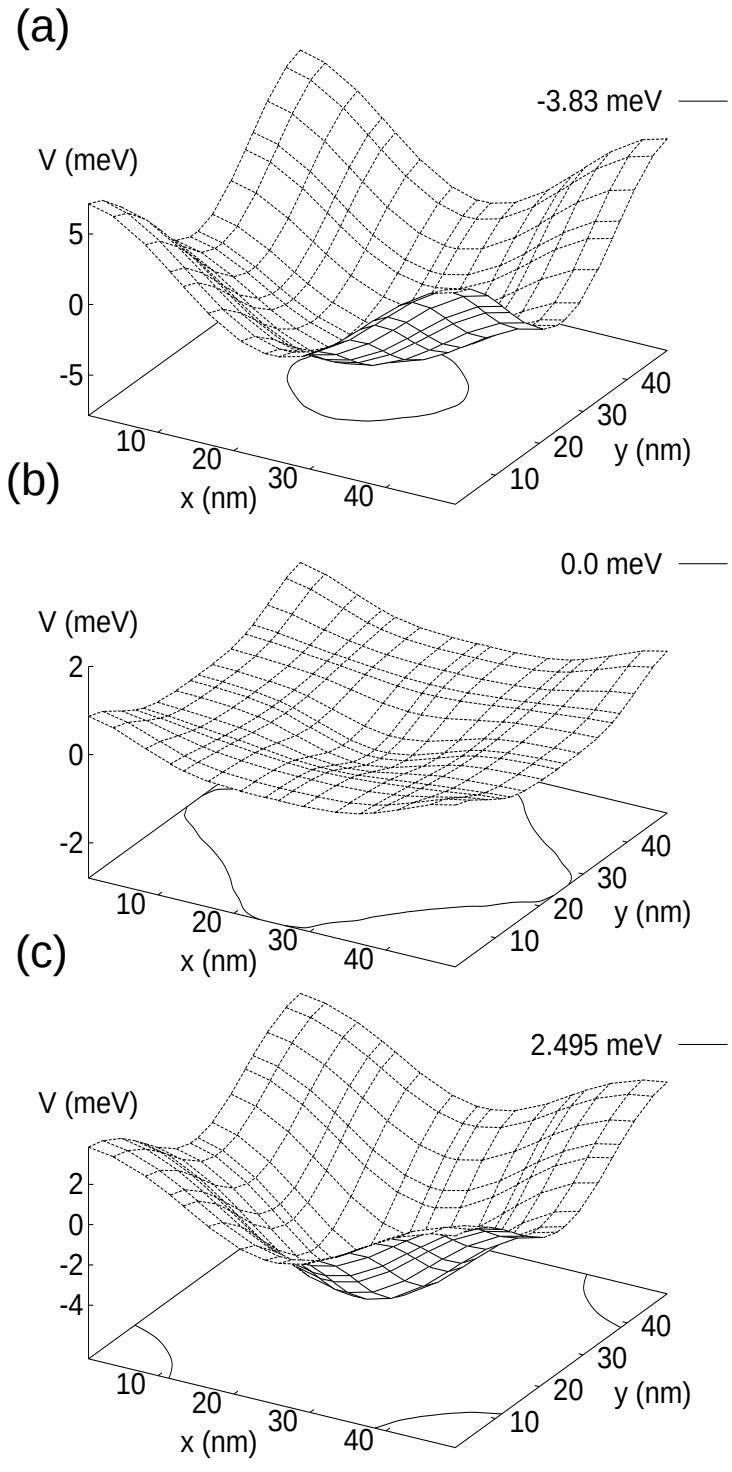

Gudmundsson, Fig. 2

(a)

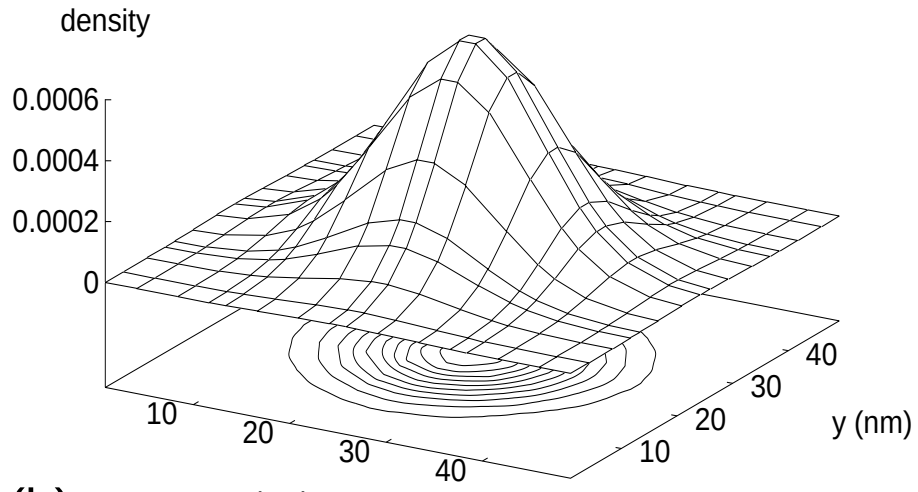

(b)

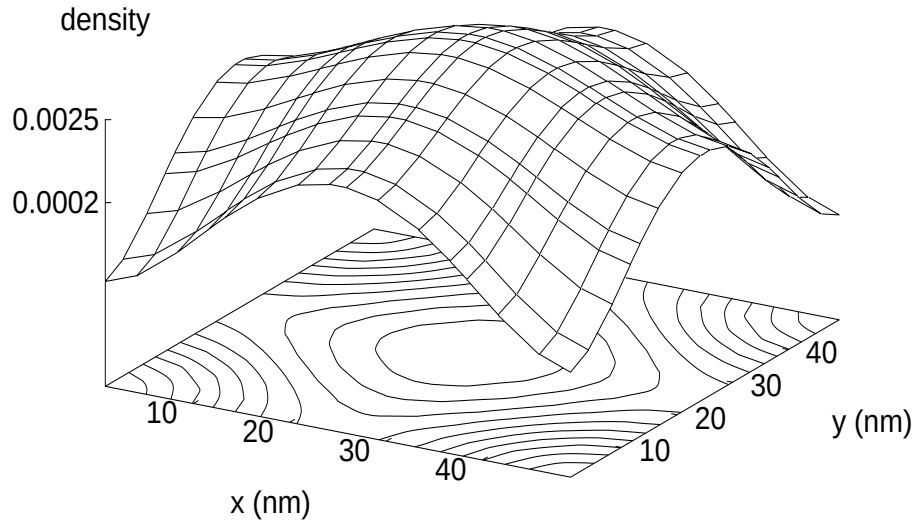

Gudmundsson, Fig. 3

(a)

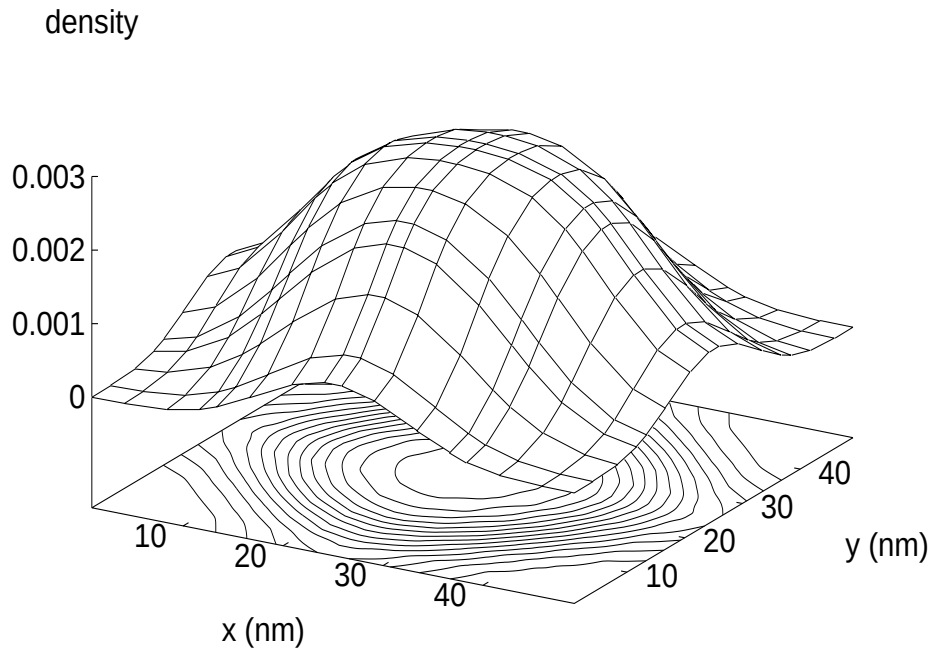

(b)

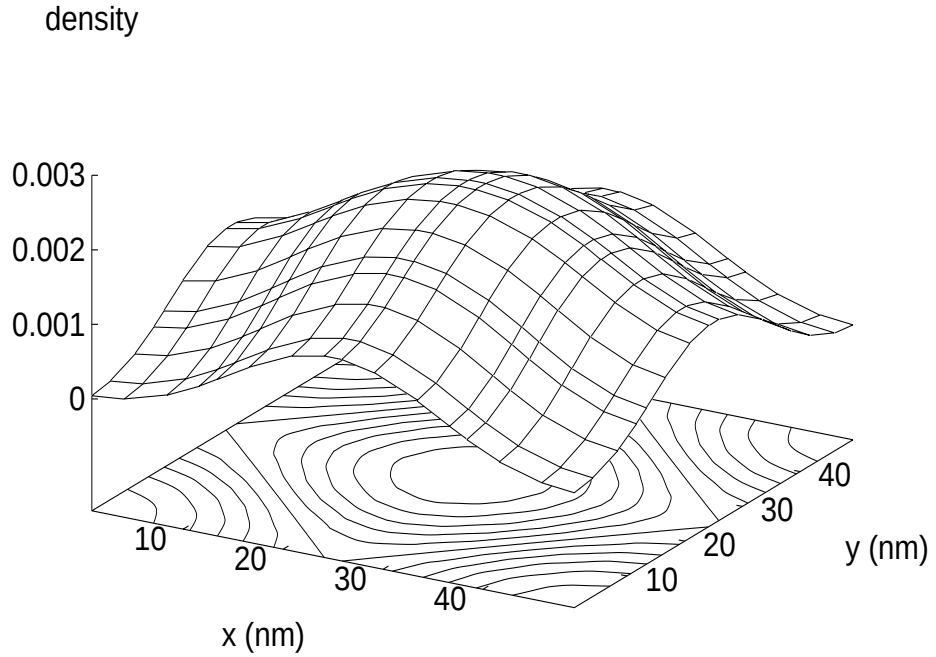

Gudmundsson, Fig. 4

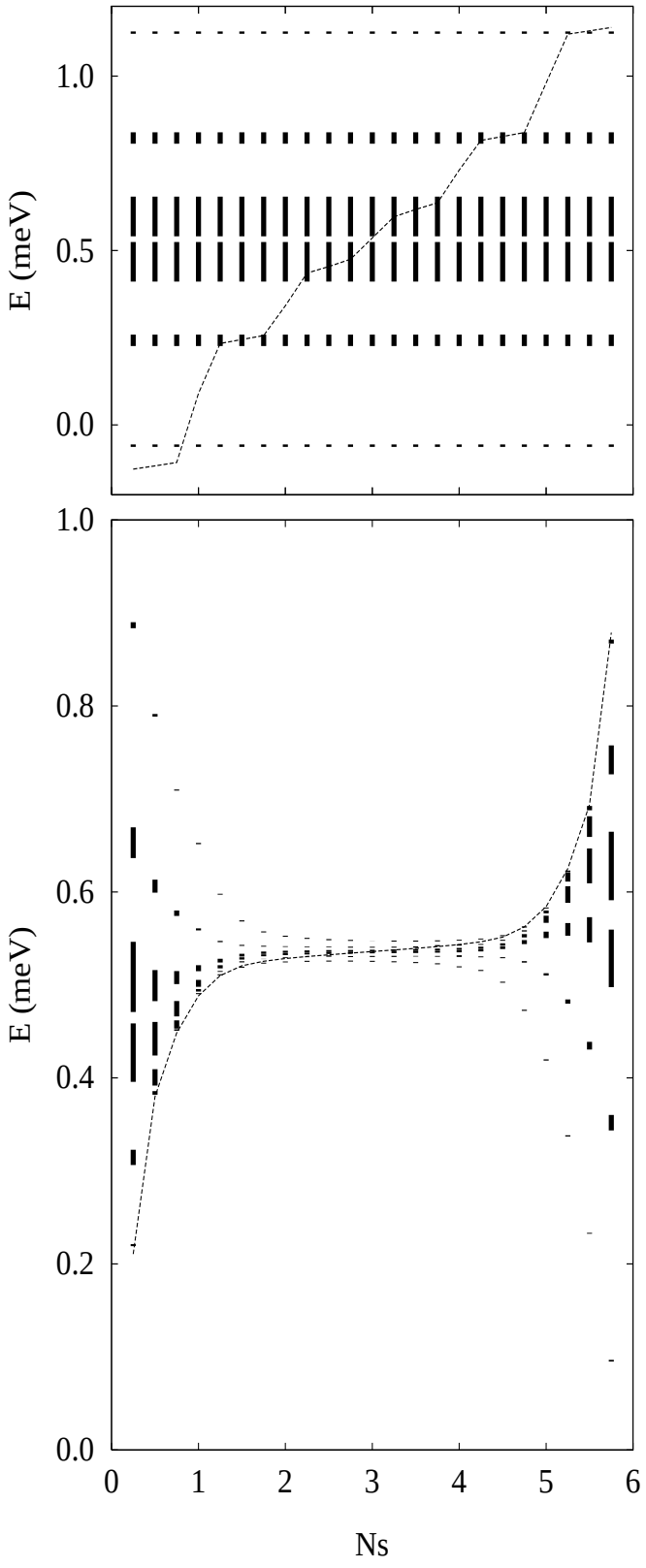

Gudmundsson, Fig. 5

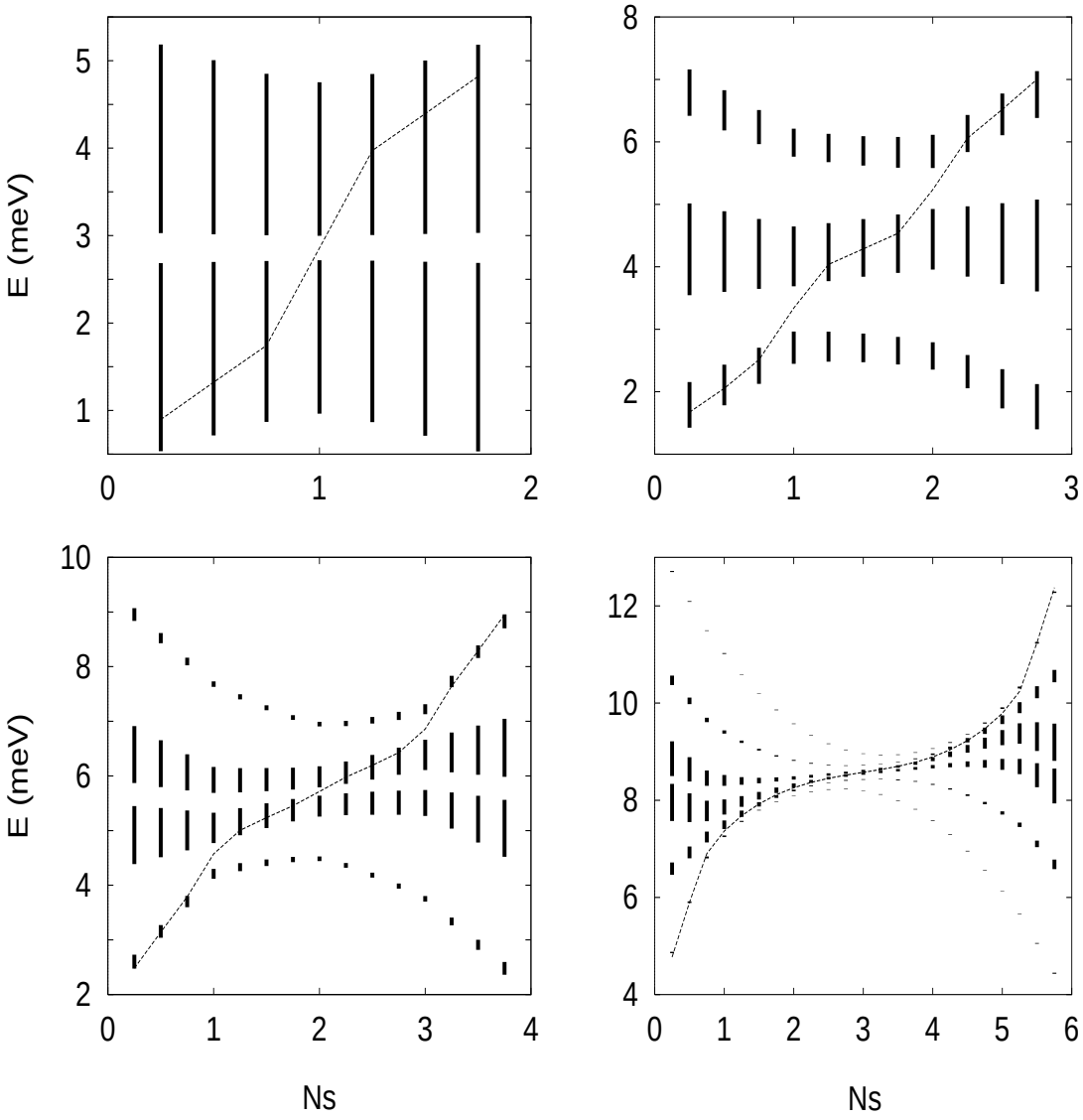

Gudmundsson, Fig. 6

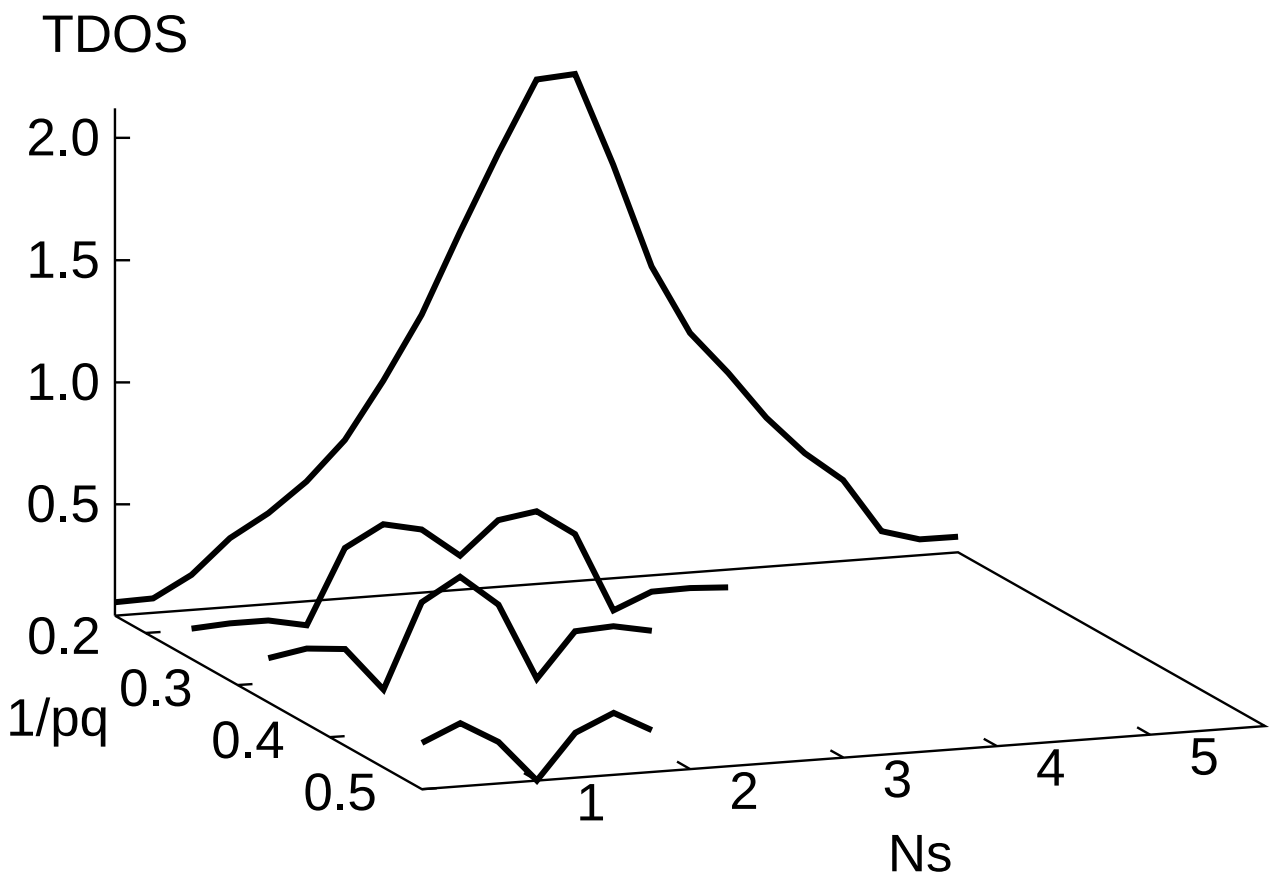

Gudmundsson, Fig. 7

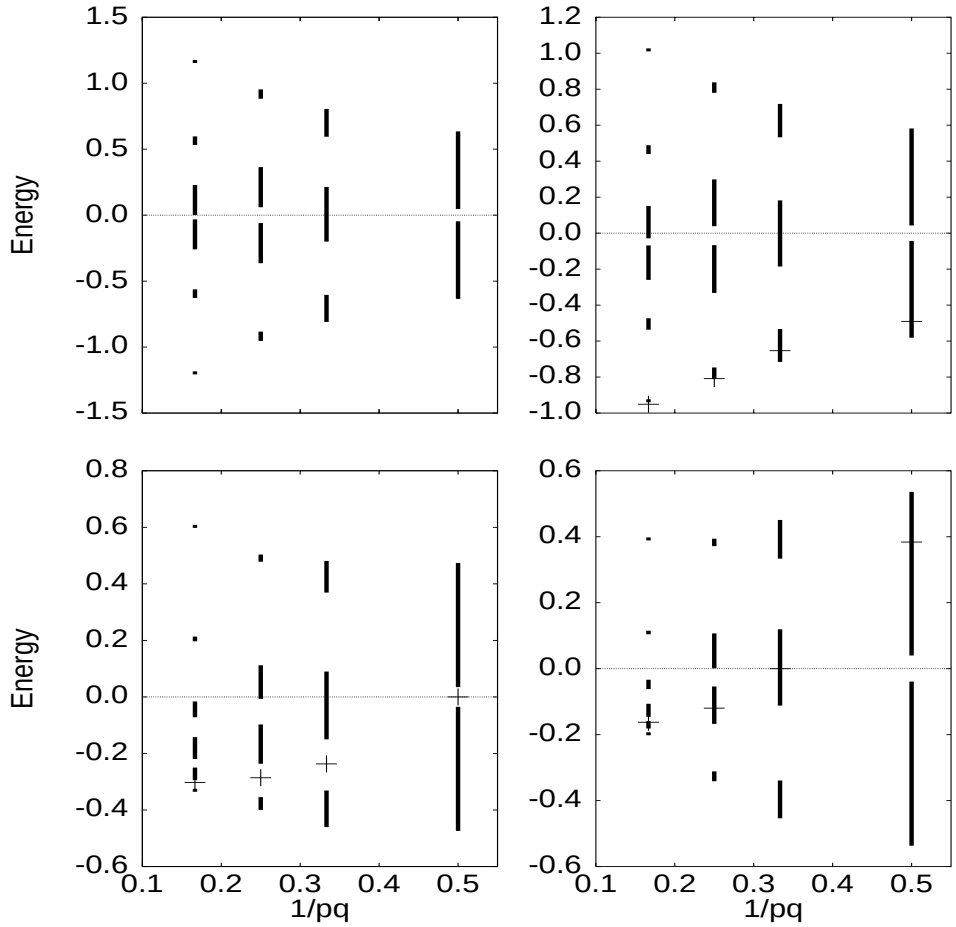

Gudmundsson, Fig. 8

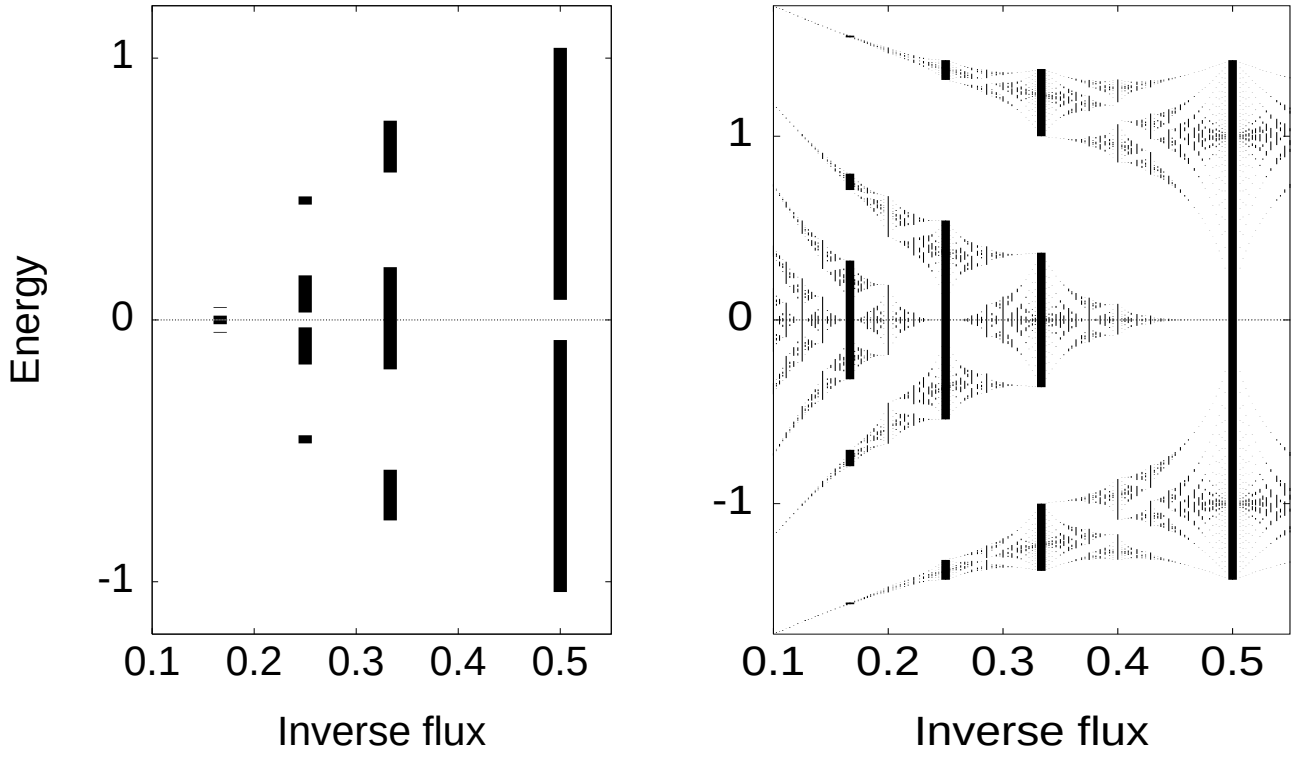

Gudmundsson, Fig. 9